

Photoelectrons and Multipacting in the LHC: Electron Cloud Build-up

G.V. Stupakov^{*,†}

Abstract

A simple quasi-analytic model is developed for the dynamics of electron cloud generated by synchrotron radiation of the beam in the LHC beam pipe. The model allows to obtain a multipacting condition for the LHC parameters, takes into account the space charge effect and predicts an equilibrium density of the electrons. Based on this model, we find the electron lifetime and estimate the energy deposition of the electron cloud to the wall. We also estimate the emittance growth of the beam due to random fluctuations of the electric field of the cloud and find the growth rate of the beam instability caused by the electrons.

*Address: Stanford Linear Accelerator Center, Stanford University, CA 94309 USA

†Member of the collaboration to the LHC project.

1 Introduction

Photoelectron production and multipacting effect in the LHC have recently become an area of intensive study [1-5]. At the beam energy of 7 TeV, the critical photon energy in a dipole magnet is 44 eV. The significant synchrotron radiation of the proton beams in the LHC will be strong enough to release a large number of photoelectrons which, if multiplied by the multipacting effect, will result in an increased energy deposition and a possible instability of the proton beam. The analysis performed so far [1, 2, 4] was mostly based on computer simulations that, with different degree of reality, take into account photoelectron production, secondary electron emission, electron dynamics, and space charge effects.

The bunch distance in the LHC is such that secondary electrons generated on the wall during a passage of a bunch with a typical energy in the range of 10 eV almost uniformly fill the vacuum chamber before the next bunch arrives. At the same time, the losses of those low-energy electrons due to the collisions with the wall are relatively small. When the next bunch arrives, it accelerates the electrons up to energies of several keV. For a secondary emission coefficient greater than unity, the number of secondary electrons produced will exceed the number of electrons accelerated by the bunch. This situation can easily lead to exponential growth of the electron cloud density up to a limit which will be determined by the space charge effects. Such beam induced multipacting was observed in the ISR ring in mid-70s [6].

The goal of this paper is to develop a simplified quasi-analytical model, that takes into account the most important effects and allows a quick analysis of the problem (though not as accurate as a computer simulation). This model shows how the electron cloud density scales with the beam characteristics, and illustrates the sensitivity of the results to the variation of the input parameters. The LHC parameters that are used in this paper are listed in Table 1.

beam energy E (GeV)	7000
number of particles in bunch N_b	10^{11}
beam current I (A)	0.54
h. r.m.s. beam size σ_x (mm)	0.2
v. r.m.s. beam size σ_y (mm)	0.2
r.m.s. bunch length σ_z (cm)	7.7
bunch spacing L_{sep} (m)	7.5
bend length l_b (m)	14.2
bend field B (T)	8.4
bending radius ρ (m)	2780
circumference C (km)	26.66
transverse emittance ε_0 (nm)	0.5
average beta function in arcs $\bar{\beta}$ (m)	88

Table 1: LHC parameters from Ref. [7].

2 Photoelectrons

The number of photons emitted by a bunch of charged particles in a bending magnetic field per unit time is $N_\gamma = 5\alpha\gamma cN_b/2\sqrt{3}\rho$ where α is the fine-structure constant, γ is the Lorentz factor, ρ is the bending radius, N_b is the number of particles in the bunch,

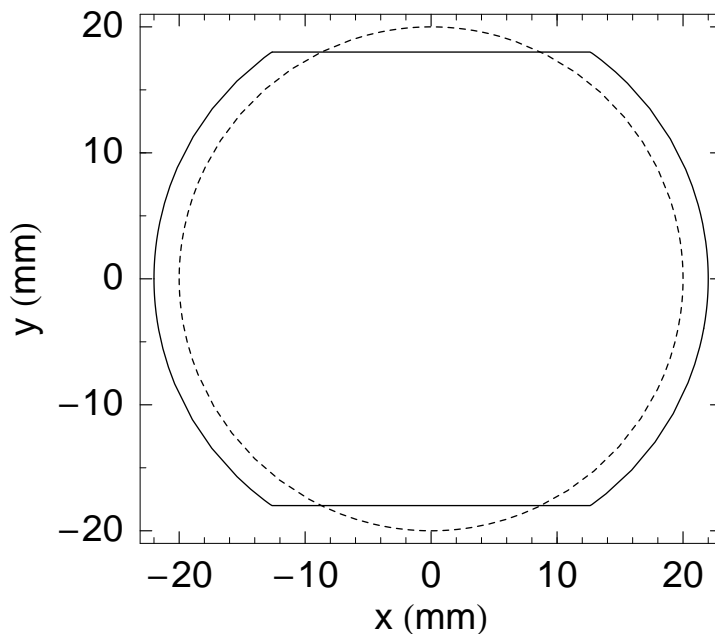


Figure 1: Cross section of the LHC screen (solid line) and a circular cross section of the pipe used in this paper (dashed line). The horizontal and vertical coordinates are denoted by x and y , respectively.

and c is the speed of light. In the LHC at 7 TeV, this amounts to about 8.5×10^{17} photons per second and per proton bunch. These photons after being emitted travel in synchronism with the bunch, and hit the wall at the time when the emitting electron is located at about the same longitudinal position in the pipe. If the one-dimensional longitudinal distribution function of the particles in the bunch is assumed Gaussian,

$$f_{part}(z, t) = \frac{N_b}{\sigma_z} \lambda\left(\frac{z - ct}{\sigma_z}\right), \quad (1)$$

where σ_z is the rms bunch length and the dimensionless function λ is

$$\lambda(\xi) = \frac{1}{\sqrt{2\pi}} e^{-\xi^2/2}, \quad (2)$$

then the distribution of the photons from a single bunch hitting the wall per unit time, per unit length and per unit azimuthal angle along the pipe cross section will be

$$n_\gamma(z, t, \phi) = \frac{N_\gamma G(\phi)}{\sigma_z} \lambda\left(\frac{z - ct}{\sigma_z}\right), \quad (3)$$

where $G(\phi)$ is a factor that gives the azimuthal distribution of the photons, $\int_0^{2\pi} G(\phi) d\phi = 1$. In what follows, we assume a circular cross section of the vacuum pipe with a radius $a = 2$ cm. The actual cross section of the screen together with the circular model used in this paper are shown in Fig. 1.

Typically, a smooth metal surface has a reflectivity close to unity for soft x-rays at grazing angles of incidence (about 5 mrad in the LHC) [8]. In this case each photon

will experience several reflections before it generates a photoelectron. Multiple reflections will uniformly distribute radiation over the pipe surface resulting in the effective function $G(\phi) \approx 1/2\pi$. We will assume a uniform irradiation in what follows.

Recent measurements at CERN, however, showed that increasing the roughness of the copper surface to about $1.6 \mu\text{m}$ suppresses the reflection coefficient down to 5% [9]. In this case, the bulk of the secondary electrons will be generated in the stripes where the synchrotron photons hit the wall, and in the most part of the accelerator the detrimental effects of the electron cloud will be strongly suppressed by the dipole magnetic field. To model the case of low reflectivity, we will introduce a reflectivity factor R in our uniform irradiation model, and assume $R \approx 1$ for large reflectivity and $R \approx 0.05$ for low reflectivity, respectively.

Each photoelectron that is generated on the wall will be accelerated by the electric field of the passing bunch. In the kick approximation which assumes that an electron does not change its radial position during the passage of the bunch, the energy of the photoelectron immediately after the passage of the bunch is given by the following formula:

$$\epsilon(z, t, \phi) = \epsilon_{max} P \left(\frac{z - ct}{\sigma_z} \right)^2 g(\phi)^2, \quad (4)$$

where for a circular pipe of radius a

$$\epsilon_{max} = 2mc^2 N_b^2 \frac{r_e^2}{a^2} \approx 200 \text{ eV}, \quad (5)$$

$P(\xi) = \int_{-\infty}^{\xi} \lambda(x) dx = \frac{1}{2} \left(1 + \text{erf}(\xi/\sqrt{2}) \right)$, m is the electron mass, and r_e is the classical electron radius. The factor $g(\phi) = 1$ in magnetic field free regions; in dipoles where the strong vertical magnetic field constrains the electron motion to the vertical direction only, one has to take a projection of the radial electric field of the beam on the vertical axis which results in $g(\phi) = \sin \phi$ (the angle ϕ is measured from the horizontal plane).

For a given distribution of the photons on the wall, Eq. (3), and the energy gain for each electron given by Eq. (4), we can find the distribution function of the photoelectrons $f_{pe}(W, \phi)$ over the energy W and the azimuthal angle ϕ after the passage of the bunch:

$$f_{pe}(W, \phi) = R \delta_{\gamma e} \int_{-\infty}^{\infty} \delta(W - \epsilon(z, t, \phi)) n_{\gamma}(z, t) dt, \quad (6)$$

where $\delta_{\gamma e}$ is the photo-yield, and δ in the integrand denotes the Dirac δ -function. The function $f_{pe}(W, \phi)$ is defined so that $f_{pe}(W, \phi) dW d\phi$ gives the number of photoelectrons left after the passage of the bunch per unit length of the pipe in the energy range $[W, W + dW]$ within the azimuthal angle $[\phi, \phi + d\phi]$. Performing the integration yields

$$f_{pe}(W, \phi) = \frac{\delta_{\gamma e} N_{\gamma}}{4\pi c g(\phi) \sqrt{\epsilon_{max} W}}. \quad (7)$$

The electron energy W in Eq. (7) varies from 0 to ϵ_{max} in the straight sections, and from 0 to $\epsilon_{max} \sin^2 \phi$ in dipoles. The inverse square root dependence on energy in Eq. (7) has been previously mentioned in Refs. [10, 11] and as a matter of fact holds for arbitrary longitudinal bunch distribution. The average energy for the photoelectrons can be easily found from Eq. (7): without magnetic field it is equal to $(1/3) \epsilon_{max} \approx 65 \text{ eV}$, and in the dipoles it is $(1/6) \epsilon_{max} \approx 30 \text{ eV}$. Electrons with such energies will cross the vacuum

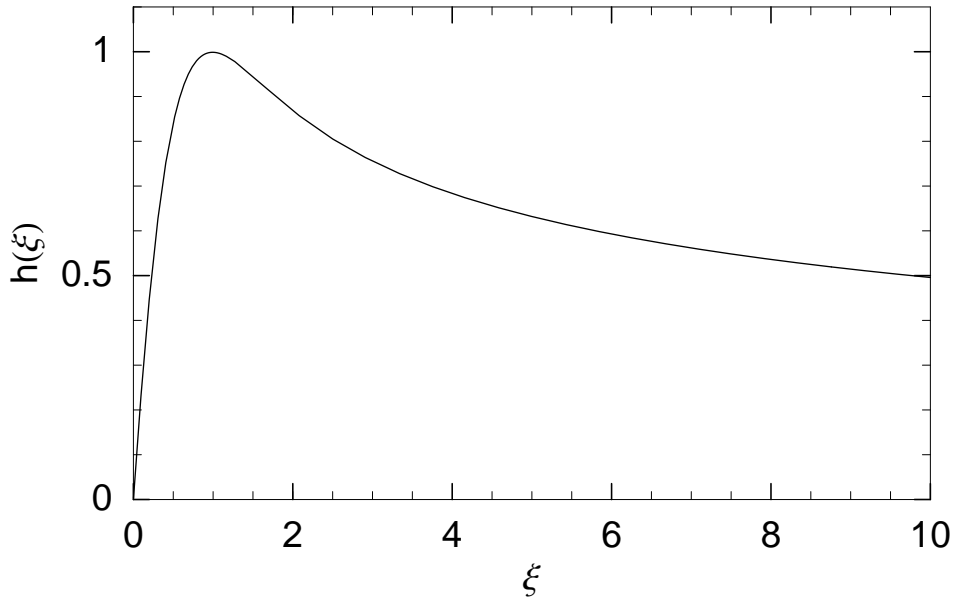


Figure 2: Normalised secondary emission function $h(\xi)$. The maximum value of h is equal to 1, and is reached at $\xi = 1$. One unit of ξ corresponds to the energy W_0 which we assume to be 400 eV throughout this paper.

chamber of about 4 cm in diameter, hit the wall and produce secondary electrons before arrival of the next bunch.

There exist different estimates of the photo-yield $\delta_{\gamma e}$ in literature varying from 0.02 in Ref. [4] to about 1.0 in Ref. [1]. Below we will use the value $\delta_{\gamma e} = 0.1$ which agrees with the last measurements performed at CERN ¹⁾ [12].

3 Secondary Electron Emission

Following Refs. [1, 13] we assume that the secondary emission yield δ_{sey} as a function of the energy of the electron W and the incidence angle θ is represented by the following formula

$$\delta_{\text{sey}}(W, \theta) \approx \frac{\delta_{\text{max}}}{\cos \theta} h\left(\frac{W}{W_0}\right), \quad (8)$$

where δ_{max} is the maximum yield, W_0 is the energy corresponding to this maximum, θ is counted from the normal to the surface, and the function $h(\xi)$ is given by the following formula

$$h(\xi) = 1.11\xi^{-0.35} (1 - e^{-2.3 \xi^{1.35}}). \quad (9)$$

The plot of the function $h(\xi)$ is shown in Fig. 2. Using the photoelectron distribution function given by Eq. (7) and the secondary electron yield, we can calculate the total number of secondary electrons generated by those photoelectrons:

$$N_{se} = \int_0^\infty dW \int_0^{2\pi} d\phi \delta_{\text{sey}}\left(W, \frac{\pi}{2} - \phi\right) f_{pe}(W, \phi), \quad (10)$$

¹⁾ The latest measurements at 11 mrad incidence angle give $\delta_{\gamma e} = 0.15$ for 1.6 μm surface roughness and $\delta_{\gamma e} = 0.21$ for 0.2 μm roughness.

where we took into account that the incidence angle $\theta = \pi/2 - \phi$. Eq. (10) gives the number of secondary electrons per unit length of the pipe generated in the magnetic field after passage of the bunch. In field-free regions one should set $\phi = \pi/2$ in the integrand on the right hand side of the equation. Assuming the value of the critical energy $W_0 = 400$ eV and performing numerical integration gives the following result:

$$\begin{aligned} N_{se} &= 0.34 R \delta_{\gamma e} \delta_{\max} \frac{N_\gamma}{c}, & \text{in straight sections,} \\ N_{se} &= 0.23 R \delta_{\gamma e} \delta_{\max} \frac{N_\gamma}{c}, & \text{in dipoles.} \end{aligned} \quad (11)$$

The smaller number of secondary electrons in the dipoles is explained by the fact that the energy gain ϵ of the photoelectrons goes down when $\phi \rightarrow 0$ causing the secondary emission yield to vanish (in spite of the $1/\cos\theta$ dependence of δ_{sey}).

Choosing the values $\delta_{\gamma e} = 0.1$ for the photoemission yield, $\delta_{\max} = 1.3$ for the secondary emission yield and $R = 1$, gives $N_{se} = 1.2 \times 10^6$ secondary electrons per centimeter in the straight sections and $N_{se} = 0.8 \times 10^6$ cm⁻¹ in dipoles. After these electrons are uniformly distributed over the pipe cross section (see below), they would produce an electron cloud with a density of about 10^5 cm⁻³ and 0.7×10^5 cm⁻³, in straight sections and dipoles, respectively.

4 Multipacting

4.1 Free Motion and Distribution Function of the Secondary Electrons

So far we have considered the electron cloud during the passage of a single bunch. Now we need to look at what happens with those electrons when subsequent bunches pass by.

Note first, that photoelectrons have relatively small average energy (30 or 65 eV, see above), and cross the distance between the walls within a time comparable to the bunch spacing of 25 ns²). That means that generation of the secondary electrons will occur rather uniformly in time between the first and the second bunches. After the second bunch arrives, it accelerates the secondary electrons up to an energy of several kiloelectronvolts and causes them to hit the wall and to be converted into the next generation of secondaries almost immediately after the passage of the bunch. The same process repeats with the passage of next bunches. We will consider below the dynamics of the electron cloud between the subsequent passage of the bunches, find the balance between the losses of the secondary electrons and their production and obtain a condition of multipacting, corresponding to unlimited growth of the cloud population.

Let us set $t = 0$ corresponding to the moment immediately after the passage of the bunch under consideration. We assume that by this time all secondary electrons are produced and sit close to the wall surface. We also assume that their velocity distribution function is given by a half-Maxwellian with a characteristic energy W_s , and all electrons are emitted perpendicular to the wall surface. The total distribution function over velocity and coordinates at $t = 0$ is

$$f_e^{(0)}(v, x, y) = n_0(x) \sqrt{\frac{2m}{\pi W_s}} e^{-mv^2/2W_s} \delta(y - y_0(x)), \quad v > 0, \quad (12)$$

where the velocity v is directed from the wall toward the axis, $y_0(x) = \pm\sqrt{a^2 - x^2}$ gives the y -coordinate of the wall for a given x , and $n_0(x)$ is the number of electrons per unit

²) A 60 eV electron passes the screen diameter of 4 cm in about 9 ns.

area in $x - z$ plane. The δ -function term reflects the fact that all electrons are initially localised on the wall. The function $f_e^{(0)}$ is defined so that when integrated over v from 0 to infinity it gives the electron density (particles per cubic centimeter) in the pipe ($n_0(x)$ has a dimension of particles per unit area), and integrated over velocity and the geometrical cross section of the pipe, it gives the total number of the secondary electrons left after the passage of the bunch:

$$\int dx dy \int_0^\infty dv f_e^{(0)}(v, x, y) = 2 \int_{-a}^a dx n_0(x) = N_e. \quad (13)$$

In the magnetic field, we can assume that particles move only in the vertical direction, their horizontal position being “frozen” within a small Larmor radius. In order to compute the dynamics of the cloud, we actually need the distribution function over the vertical component of the velocity $v_y = vy_0/a$ which can be found from Eq. (12),

$$f_e^{(0)}(v_y, x, y) = \frac{2an_0(x)}{v_s y_0(x)} \lambda \left(\frac{v_y a}{v_s y_0(x)} \right) \delta(y - y_0(x)), \quad (14)$$

where $v_s = \sqrt{W_s/m}$ and λ is given by Eq. (2).

In the course of the free motion of the electrons until the next bunch arrives, v_y remains constant and $y = y_0(x) + v_y t$. Using the fact that the distribution function of a Hamiltonian system is a function of integrals of motion, we can easily find it at time $t > 0$:

$$f_e(v_y, x, y, t) = f_e^{(0)}(v_y, x, y - v_y t). \quad (15)$$

Integrating this formula over v_y gives the density of the electrons at time t ,

$$n_e(x, y, t) = \frac{2an_0(x)}{tv_s y_0(x)} \left[\lambda \left(\frac{y - y_0(x)}{tv_s y_0(x)} \right) + \lambda \left(\frac{y + y_0(x)}{tv_s y_0(x)} \right) \right]. \quad (16)$$

The two terms in Eq. (16) account for the electrons that move along the field line from the upper and lower parts of the walls, respectively. The scaled density distribution in the symmetry plane $x = 0$ for $W_s = 10$ eV at different times is shown in Fig. 3.

Integration of the density Eq. (16) along the field line gives the number of particles in the pipe as a function of time. This number decreases with time because particles get lost when they hit the wall. In reality, the particles that reach the wall can produce secondary electrons, however the secondary emission yield in the range of 10 eV is small and this effect can be neglected. The relative number of particles lost by the time t is

$$\delta_{\text{loss}}(x, t) = 1 - \frac{1}{n_0(x)} \int_0^{y_0(x)} n_e(x, y, t) dy. \quad (17)$$

Numerical integration gives $\delta_{\text{loss}} = 0.23$ for $t = 25$ ns and $W_s = 10$ eV (it is easy to see from Eqs. (16) and (17) that δ_{loss} actually does not depend on x ³⁾). The dependence of δ_{loss} on W_s is shown in Fig. 4.

The filling pattern in the LHC assumes that the beam is divided into batches of 81 bunches separated by the gaps of 220 or 940 ns [7]. Using Eq. (17) we find $\delta_{\text{loss}} = 0.88$ for $t = 220$ ns and $\delta_{\text{loss}} = 0.97$ for $t = 940$ ns.

³⁾ This is a consequence of our assumption of circular pipe cross section.

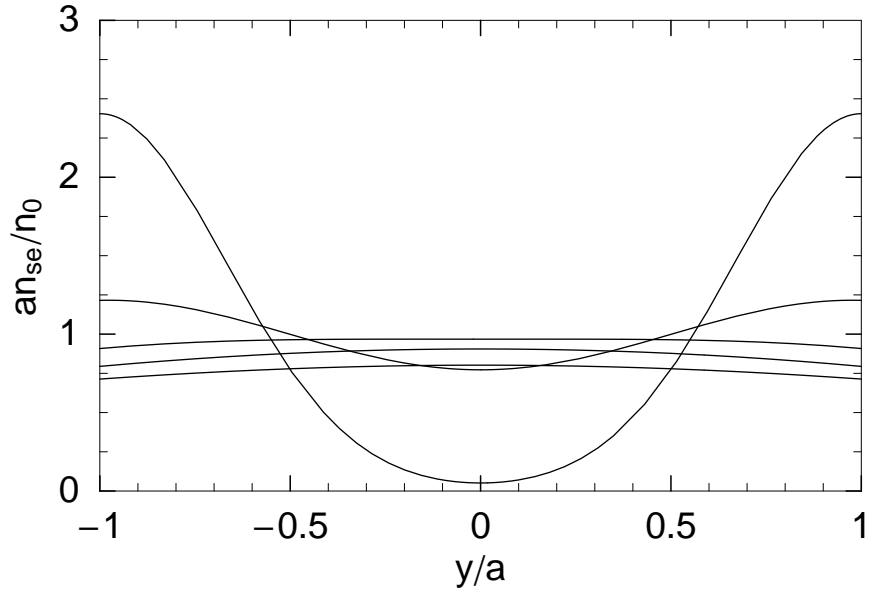


Figure 3: Scaled density $an_e(0, y, t)/n_0(0)$ of the secondary electrons in the vertical symmetry plane at five different times $t = 5, 10, 15, 20$ and 25 ns. The initial double-Gaussian profile smooths out into almost uniform distribution along the field line after about 10 ns.

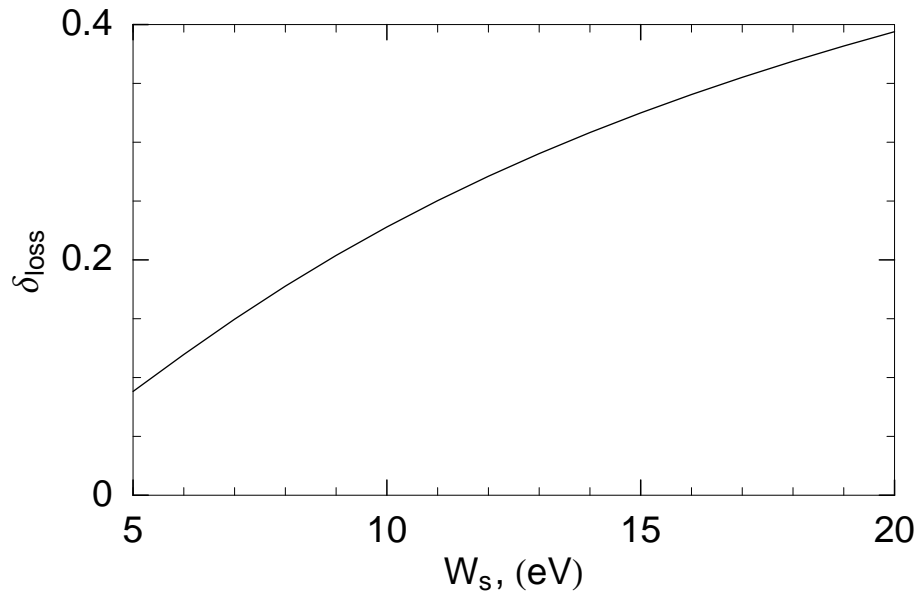


Figure 4: Fraction of secondary electrons lost between the bunches as a function of their characteristic energy W_s .

4.2 Acceleration of Secondary Electrons by the Beam and Multipacting Condition

At time $t_{\text{sep}} = L_{\text{sep}}/c = 25$ ns the next bunch arrives, and the secondary electrons distributed according to Eq. (16) get a kick from the electric field of this bunch. Accelerated up to energies of several kiloelectron-volts they will quickly get to the walls and create a new generation of secondary electrons. If the number of new secondary electrons, $n_1(x)$, is larger than the initial number $n_0(x)$, we will have an exponential growth of the secondary electrons with the passages of subsequent bunches (in the absence of the space charge effect). In the opposite case, the initial group of photoelectrons will exponentially decay after several cycles.

In order to find the threshold for multipacting we need to calculate the energy of the electrons which fill the pipe, after the passage of the next bunch, and find the number of the new generation secondary electrons after they hit the wall. For this calculation, again we will assume a kick approximation for the energy gain. For an electron located at position x, y , the kick energy gain is

$$W(x, y) = \epsilon_{\text{max}} \frac{y^2 a^2}{(x^2 + y^2)^2}. \quad (18)$$

In this expression we used the fact that the bunch electric field varies inversely proportional to the distance and included the projection of the electric field on the magnetic field line. This energy as a function of y is shown in Fig. 5 for several horizontal coordinates x .

As shown in Ref. [11], the kick approximation fails for an energy gain W exceeding 1–1.5 keV. We see from Fig. 5, however, that this range of energies corresponds to a relatively small area in the physical space limited by $y < 0.5a$ and $x < 0.2a$. Noting that the secondary emission coefficient is a smooth function of the energy for 1–2 keV, we expect that the error produced by the kick approximation is not essential for our problem.

Similar to Eq. (10), we can now calculate the number of new generation secondary electrons that are produced after the passage of the second bunch

$$n_1(x) = \int dy \delta_{\text{sey}}(W(x, y), \theta) n_e(x, y, t_{\text{sep}}), \quad (19)$$

where t_{sep} is the time interval between the bunches and the angle θ is related to x through $\cos \theta = y_0(x)/a$. As mentioned above, if the ratio $n_1(x)/n_0(x)$ is greater than 1, the multipacting occurs. Using Eq. (19), the condition for the multipacting can be written as

$$\delta_{\text{max}} > \delta_{\text{crit}}(x) \equiv \left(\int dy h(W(x, y)) \frac{a}{y_0(x)} \frac{n_e(x, y, t_{\text{sep}})}{n_0(x)} \right)^{-1}. \quad (20)$$

Note that in the magnetic field δ_{crit} varies from one magnetic field line to another. Numerically calculated values of δ_{crit} are plotted in Fig. 6 for several values of W_s . As we see, the lowest values of δ_{crit} is reached at the values of x/a between 0.2 and 0.4.

4.3 Build-up of Electron Cloud

Let us assume that the actual secondary emission yield is larger than the critical one, $\delta_{\text{max}} > \delta_{\text{crit}}$. In this case, a group of electrons initially produced by a single bunch is amplified after each passage of subsequent bunches by a factor $1 + q$, where

$$q = |\delta_{\text{max}}/\delta_{\text{crit}} - 1|, \quad (21)$$

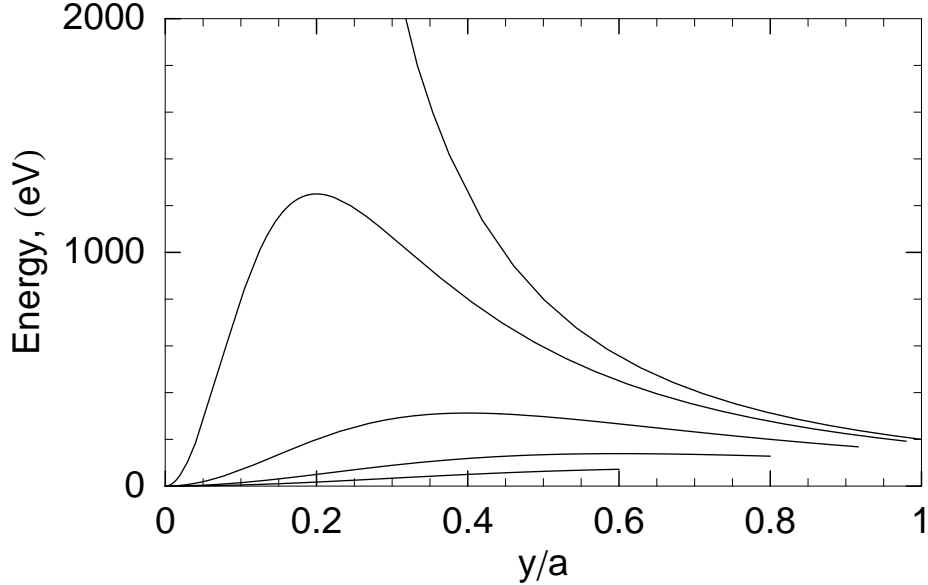


Figure 5: Energy gained by an electron after passage of the proton bunch as a function of the vertical coordinate y for different values of x , $x/a = 0, 0.2, 0.4, 0.6$, and 0.8 (smaller x correspond to the curves with higher energies.)

which means an exponential growth $N_e \approx N_{se} \exp(tq/t_{sep})$. In addition to amplifying the existing electron cloud, each bunch adds its own secondary electrons generated by photoelectrons. We can find the total density of the cloud after the passage of $M = t/t_{sep}$ bunches by summing contributions from every bunch. Note that the electron density N_{se} generated by the k th bunch immediately after the passage by the time of observation will be amplified by a factor of $\exp[q(M - k)]$. The total density from all bunches is

$$N_e = \sum_{k=1}^M N_{se} e^{q(M-k)} = N_{se} \frac{e^{Mq} - 1}{e^q - 1} \approx \frac{N_{se}}{q} e^{tq/t_{sep}}, \quad (22)$$

where in the last formula we assumed that $q \ll 1$ and $Mq \gg 1$. Unlimited growth predicted by Eq. (22) will eventually be stopped by the space charge effect (see below).

If the multipacting condition is not satisfied, $\delta_{max} < \delta_{crit}$, then an initial electron cloud will decay as $N_{se} \approx \exp(-tq/t_{sep})$. Adding contributions to the cloud from other bunches results in a steady state density of the electron cloud at the level

$$N_e = \sum_{k=1}^{\infty} N_{se} e^{-qk} = N_{se} \frac{1}{e^q - 1} \approx \frac{N_{se}}{q}, \quad (23)$$

which means that for a small q there may be a substantial increase in the electron density compared to the electron cloud for a single bunch. Of course, if the density given by Eq. (23) is so large that the space charge effects play a role, then the space charge effects will actually limit the density before it reaches equilibrium predicted by Eq. (23).

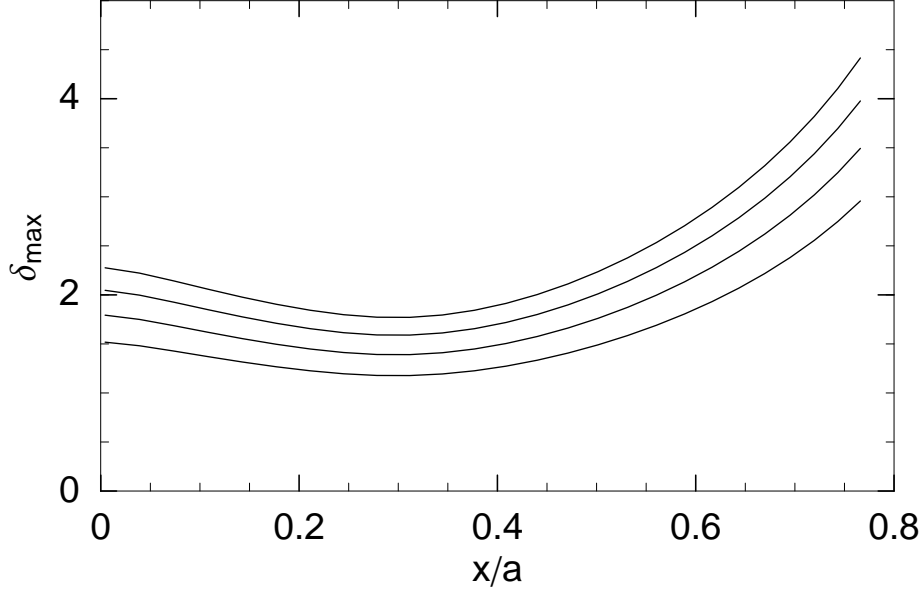


Figure 6: Critical value of the maximum secondary electron yield δ_{\max} as a function of x for different characteristic energies $W_s = 5, 10, 15$ and 20 eV of the secondary electrons. Higher energy corresponds to larger δ_{crit} .

It is important to emphasise here that in both cases the characteristic time that determines the development of the electron cloud is the same

$$\tau_e = \frac{t_{\text{sep}}}{q}. \quad (24)$$

For not very small q , this means that the cloud reaches equilibrium after the passage of several bunches.

5 Space Charge Effects

A simple estimate of the electron cloud density at which the space charge effects become important is given by the Debye radius of the electron cloud [14]

$$r_D = \sqrt{\frac{W_s}{4\pi n_e e^2}}, \quad (25)$$

where we approximate the thermal energy of the electrons by W_s . If the density is such that the Debye radius becomes comparable to the pipe radius, the electric field of the space charge will effectively decelerate the electrons when they are moving away from the wall toward the center, and push them back into the wall surface preventing the further buildup of the cloud. We have to emphasise here that this mechanism limits the electron cloud density to a level that depends (for a given bunch spacing) only on the average energy of the emitted secondary electrons W_s and on the pipe radius a . It is not related

to the charge of the proton bunch, contrary to the statement of Ref. [1]. Equating r_D to the pipe diameter $2a$ gives a rough estimate for the maximum electron density

$$n_{\max} \approx \frac{W_s}{\pi a^2 e^2} \approx 6 \times 10^6 \text{ cm}^{-3}. \quad (26)$$

Note that this density corresponds to a number of electrons in each dipole magnet equal to 10^{11} .

A full self-consistent treatment of the space charge effects is a complicated problem that should take into consideration the nonaxisymmetric time-dependent electric field generated by the cloud in the pipe and the dynamics of the secondary electrons. A detailed treatment of the problem is only available numerically, however, the main mechanism of the space charge effect can be understood with the help of a simplified analytical model.

Let us consider the case without magnetic field, when the problem is axisymmetric. First, we can calculate the electric field on the wall E at time $t = 0$, when the secondary electrons are all located close to the wall, as $E = 2eN_e/a$, where N_e is the number of secondary electrons in the pipe per unit length. This electric field on the wall remains constant at $t > 0$ if one neglects particle losses. In our model we compute the motion of the electrons and their distribution function assuming that *all* electrons are affected by the electric field E .

The electron motion in the radial direction with initial location r_0 (equal to the pipe radius) and with initial velocity v_0 , in the constant electric field is

$$v = v_0 + \frac{eE}{m}t, \quad r = r_0 + v_0t + \frac{eE}{2m}t^2. \quad (27)$$

The initial distribution function in the axisymmetric system is a straightforward generalisation of Eq. (12),

$$f_e^{(0)}(v, r) = N_e \sqrt{\frac{2m}{\pi W_s}} e^{-mv^2/2W_s} \delta(r - a) = \frac{2N_e}{v_s} \lambda\left(\frac{v}{v_s}\right) \delta(r - a), \quad v > 0, \quad (28)$$

where a positive value of v corresponds to the motion toward the axis. This function is now defined so that $\int_0^a dr \int_0^\infty dv f_e = N_e$. Using Eq. (27) and the fact that the distribution function is constant along particle's orbit, we can find the distribution function at time t

$$f_e(v, r, t) = f_{se}^{(0)}\left(v - \frac{eEt}{m}, r - vt + \frac{eEt^2}{2m}\right), \quad (29)$$

and integrating f_e over v gives

$$\hat{n}_e(r, t) = \frac{2N_e}{tv_s} \left[\lambda\left(\frac{r-a}{tv_s} - \mathcal{E}\right) + \lambda\left(\frac{r+a}{tv_s} + \mathcal{E}\right) \right], \quad (30)$$

where $\hat{n}_e(r, t)dr$ gives the number of electrons per unit length of the pipe located within $[r, r + dr]$ ⁴. The dimensionless electric field \mathcal{E} in Eq. (30) is

$$\mathcal{E} = \frac{eEt}{2mv_s} = \frac{e^2 N_e t}{mv_s a}. \quad (31)$$

For $\mathcal{E} = 0$, Eq. (30) reduces to Eq. (16) in which $x = 0$ (the vertical symmetry plane).

⁴ The electron density n_e is expressed in terms of \hat{n}_e as $n_e = \hat{n}_e/2\pi r$.

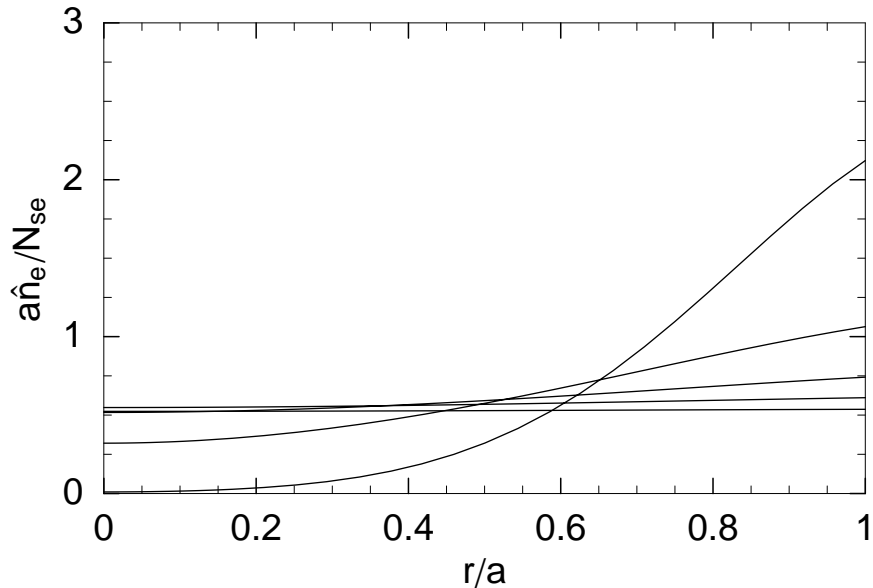


Figure 7: Scaled density $a\hat{n}_e(r, t)/N_e$ of the secondary electrons for $\mathcal{E} = 0.5$ at five different times $t = 5, 10, 15, 20$ and 25 ns. Compare with Fig. 3.

Eq. (30) describes propagation and redistribution of the secondary electrons in the pipe with account of the space charge effect. For illustration of the electric field effect, we plot in Fig. 7 the density \hat{n}_e for $\mathcal{E} = 0.5$ and $t = t_{\text{sep}}$. Comparing this figure with Fig. 3, we see that electric field lowers the final density of the electrons, causing additional losses of the particles. The fraction of particles lost on the walls at $t = t_{\text{sep}}$ is 0.47 which is more than two times larger than without electric field (see Section 4.1). For $t = t_{\text{sep}}$ and $W_s = 10$ eV, one unit of \mathcal{E} corresponds to $N_e = 4.2 \times 10^7 \text{ cm}^{-1}$, or a density $n = 3.3 \times 10^6 \text{ cm}^{-3}$ of uniform distribution.

Using the distribution function (30) we can now recalculate the critical secondary emission coefficient δ_{crit} , which becomes a function of \mathcal{E} , paralleling the calculations of section 4.2. The result of such calculation is shown in Fig. 8 for several energies W_s . As is seen from this figure, increasing \mathcal{E} results in larger values of δ_{crit} , because, as mentioned above, the electric field pushes the low energy particles onto the wall and increases the loss of the secondary electrons.

Recalling now the electron cloud dynamics from section 4.3, we arrive at the following scenario of development of the electron cloud. If the secondary electron coefficient δ_{max} is initially greater than δ_{crit} , an exponential growth of the electron cloud occurs. With the growth of N_e , the value δ_{crit} increases in accordance with Fig. 8 until it exceeds δ_{max} . At some point, the exponential growth of the cloud stops and the losses become such that they exactly compensate the supply of new electrons from passing bunches. The equilibrium level can be computed using Eq. (23) in which q has to be calculated with account of the electric field:

$$N_e \left(1 - \frac{\delta_{\text{max}}}{\delta_{\text{crit}}(\mathcal{E}(N_e))} \right) = N_{se}. \quad (32)$$

We remind here that in this equation N_e is the equilibrium linear density of the cloud and

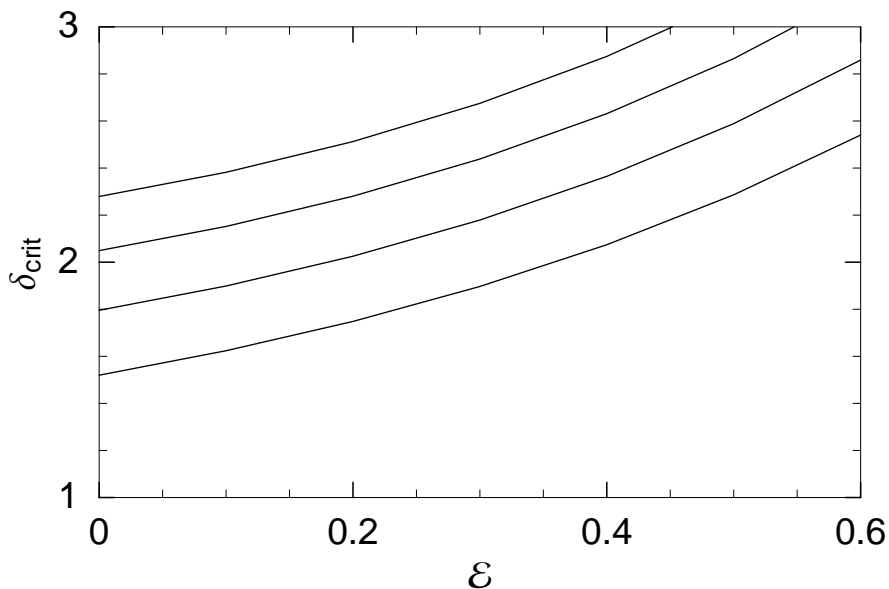


Figure 8: Critical value δ_{crit} of the maximum secondary electron yield as a function of dimensionless electric field \mathcal{E} for $x = 0$ and $W_s = 5, 10, 15$ and 20 eV. Larger W_s correspond to higher values of δ_{crit} .

N_{se} is the linear density generated by a single bunch.

For illustration, we assume that $\delta_{\text{max}} = 2$, and take $N_{se} = 10^6 \text{ cm}^{-1}$. Then solving numerically Eq. (32) we find that in equilibrium $\mathcal{E} = 0.30$, and $N_e = 1.24 \times 10^7 \text{ cm}^{-1}$ which corresponds to a uniform electrons density $n_e = 1.0 \times 10^6 \text{ cm}^{-3}$, or 1.7×10^{10} electrons per dipole magnet.

6 Energy Deposition to the Wall

Every time after a passage of a bunch all electrons in the pipe hit the material surface and deposit their kinetic energy into the wall. To estimate the heat load due to this effect we cannot use Eq. (18) because it overestimates the energy gain for electrons close to the beam ⁵⁾. Instead, we will use a result of computer simulation, that shows that the average energy deposited by each electron in dipoles for the nominal parameters of the LHC is approximately equal to 300 eV [2, 4]. With this number, we can first estimate the energy deposition corresponding to the first generation secondary electrons produced by each bunch. The linear density of these electrons, for $R = 1$, is given by Eq. (11), and for $N_{se} = 10^6 \text{ cm}^{-1}$ one finds the head load $P = 0.44 \text{ W/m}$. For a reflection coefficient $R = 0.05$, the density N_{se} and the power load P become 20 times smaller.

However, due to the secondary emission of electrons, the equilibrium electron density N_e is always higher than N_{se} . In case when the multipacting condition is not satisfied, N_e is given by Eq. (23). According to Fig. 6, the minimum value of δ_{crit} for $W_s = 10$ eV is equal to 1.4. Assuming $\delta_{\text{max}} = 1.1$, that is there is no multipacting in the system, we find $q = 0.2$, which means that the equilibrium density $N_e \approx 5N_{se}$, and the corresponding

⁵⁾ Formal calculation of the deposited energy using the function $W(x, y)$ would result in an integral that diverges at small x and y .

energy deposition is $P = 2.2 \text{ W/m}$ for $R = 1$ and $P = 0.11 \text{ W/m}$ for $R = 0.05$.

For a secondary emission coefficient greater than δ_{crit} , the equilibrium density is determined by the space charge effect. In this regime, the stationary density of the electron cloud does not depend on q , and is approximately equal to $N_e \approx 2 \times 10^7 \text{ cm}^{-3}$. The energy deposition corresponding to this density is almost 20 times larger than estimated for N_{se} , $P \approx 9 \text{ W/m}$.

7 Beam Emittance Growth Due to the Field of the Electron Cloud

Due to the dynamic nature of the electron cloud regenerated after passage of each bunch, we can assume that the electric field of its space charge will have a random component which fluctuates both in space and time. Random variations in space can be caused by uncontrolled changing of the secondary emission coefficient from point to point. Fluctuations in time may be related to the beam noise excited, e.g., by a feedback system. As a result, a fraction of the total electric field of the cloud will randomly change its value and orientation along the beam path producing random kicks on the beam and driving its betatron oscillations. These oscillations, after decohering, will be transformed into an increased beam emittance. The whole process is analogous to the mechanism of emittance growth due to the ground motion, where a random motion of quadrupole magnets produces uncorrelated kicks to the beam and causes constant emittance growth proportional to the square of the amplitude of the ground motion (see, e.g., Ref. [15]).

To quantitatively estimate this effect, note first that the transverse field E of the electron cloud in the pipe is of the order

$$E \sim 4\pi e a n_e. \quad (33)$$

We will assume that a small fraction f of the total field E fluctuates stochastically and use the theory from Ref. [15] to compute the emittance growth. An important parameter of the theory is a correlation length l_c , such that within each interval l_c values of the field in different points are correlated, and in regions separated by a distance larger than l_c the fields are statistically independent.

According to Ref. [15], the emittance growth due to the passage of the beam through M uncorrelated regions of length l_c of the perturbed field fE is given by the following formula ⁶⁾

$$\Delta\varepsilon = \frac{1}{2} M \bar{\beta} \left(\frac{e l_c f E}{\gamma m_p c^2} \right)^2, \quad (34)$$

where $\bar{\beta}$ is the average beta-function, and m_p is the classical proton radius. Assuming that the secondary electrons and the random field fE are present on the whole circumference of the machine, we can estimate M as the number of correlated regions passed by the beam during time t , $M = ct/l_c$, which gives the following formula for the rate of emittance growth:

$$\frac{d\varepsilon}{dt} = \frac{c}{2l_c} \bar{\beta} \left(\frac{e l_c f E}{\gamma m_p c^2} \right)^2 = \frac{c}{2l_c} \bar{\beta} \left(\frac{4\pi e^2 a n_e l_c f}{\gamma m_p c^2} \right)^2. \quad (35)$$

Finally, we define the emittance doubling time as

$$\tau_{\text{emit}} = \varepsilon_0 \left(\frac{d\varepsilon}{dt} \right)^{-1} = \frac{c\varepsilon_0}{2l_c \bar{\beta}} \left(\frac{\gamma}{4\pi r_p a n_e f} \right)^2, \quad (36)$$

⁶⁾ In equations of Ref. [15] we substitute the perturbation of the magnetic field δB by the transverse electric field fE , which is valid for a relativistic beam.

where ε_0 is the nominal beam emittance.

Without detailed knowledge of all noise sources in the ring it is impossible to make a realistic estimate of the parameters f and l_c . Let us assume, rather arbitrarily, that the electric field fluctuates at a level of 1%, $f = 0.01$, and take for l_c the diameter of the beam pipe 4 cm. For $n_e = 10^6 \text{ cm}^{-3}$, this gives an emittance doubling time

$$\tau_{\text{emit}} = 3.7 \times 10^5 \text{ sec} \approx 100 \text{ hours}, \quad (37)$$

which is large enough not to effect the collider luminosity. Note however, that choosing a larger l_c ⁷⁾ and n_e could easily decrease τ_{emit} down to a few hours.

With all its uncertainty, the estimate (37) indicates an additional potential problem associated with a high density electron cloud – a possible emittance growth of the beam.

8 Instability

8.1 A Crude Estimate

The electron cloud plays the role of a medium that keeps memory about transverse positions of bunches and carries interaction from one bunch to another. This can cause a multibunch instability of the beam similar to the Ohmi instability of a positron beam [16, 1]. Before going to details and assumptions of the model, let us make a crude estimate of the growth rate of the instability. In this paper, we limit our consideration by a horizontal instability only, which according to Ref. [1] is faster than the vertical one.

Assume that one of the bunches is offset in the horizontal direction by Δx . Due to asymmetry of its electric field, regeneration of the electron cloud will produce an asymmetric density component which will cause a horizontal dipole electric field ΔE . For a rough estimate we may assume that the perturbation of the electric field is proportional to the relative bunch offset

$$\Delta E \sim \kappa E \frac{\Delta x}{a} \sim 4\pi\kappa e n_e \Delta x, \quad (38)$$

where κ is a numerical factor, and we used Eq. (33) for the electric field.

Now, if we divide the acceleration of a proton under the influence of this electric field, $e\Delta E/m_p\gamma$, by its transverse velocity $\omega_\beta\Delta x$ associated with the betatron oscillations with the amplitude Δx , we get a crude estimate of a possible instability growth rate γ_{inst}

$$\gamma_{\text{inst}} \sim \frac{4\pi\kappa e^2 n_e}{m_p \gamma \omega_\beta}. \quad (39)$$

Putting in this equation $n_e = 10^6 \text{ cm}^{-3}$ gives $\tau_{\text{inst}} = \gamma_{\text{inst}}^{-1} = 18\kappa^{-1} \text{ msec}$. We will see below that a more accurate evaluation of the electric field gives a growth rate corresponding to $\kappa \approx 0.1$.

8.2 Wakefield of the Bunch

We will now calculate more accurately the electric field produced by a displaced bunch in a dipole magnetic field assuming that the bunch is displaced horizontally. A mechanism responsible for the generation of an asymmetric component of the density is following. A perturbed electrostatic potential of the displaced bunch results in the

⁷⁾ In the worst case, one can expect fluctuations of the electric field with the correlation length of the order of the bend magnet length 14 m.

perturbation of the energy gain for secondary electrons. Since the secondary emission yield is a function of the energy of incident electrons, this will result in a perturbation of the cloud density. An asymmetric cloud density perturbation will produce a horizontal electric field on the orbit.

Using Eq. (18) we find a perturbation of the energy gain due to the beam offset:

$$\Delta W = \frac{\partial W}{\partial x} \Delta x = -\Delta x \varepsilon_{\max} \frac{4xy^2 a^2}{(x^2 + y^2)^3}, \quad (40)$$

and a corresponding perturbation of the electron density $\Delta n_1(x)$ after accelerated electrons hit the wall (see Eq. (19)):

$$\Delta n_1(x) = \int n_e \Delta W \frac{\partial \delta_{\text{sey}}(W(x, y), \theta)}{\partial W} dy, \quad (41)$$

where n_e is the electron density (particles per cm^3) at the arrival time of the next bunch. Note that Δn_1 is a surface density; it gives a number of electrons per unit area in x - z plane. It was shown in Section 4, that the density n_e is uniform along field lines, but it varies in horizontal directions from one field line to another. We, however, neglect this variation here and assume that n_e is constant throughout the cross section of the pipe, so that

$$n_e = \frac{N_e}{\pi a^2}, \quad (42)$$

where N_e is the number of electrons in the cloud per unit length. With this assumption, the integral (41) was calculated numerically and the normalised surface density perturbation $\Delta n_1(x)a^2/N_e\Delta x$ is shown in Fig. 9. It is interesting to note that $\Delta n_1(x)$ changes sign when x varies from 0 to a ; this means that the contributions of the positive and negative perturbations of the density to the perturbation of the electric fields will partially cancel each other.

By the time of arrival of the next bunch, the surface density $\Delta n_1(x)$ will be uniformly distributed along a field line. Dividing $\Delta n_1(x)$ by the length of the field line $2\sqrt{a^2 - x^2}$, we find the perturbation of the density of the electron cloud and using the result of Appendix A we calculate the x -component of the electric field at the center of the pipe ΔE_x . This gives the following equation for ΔE_x

$$\Delta E_x = -2e \int_{-a}^a dx \Delta n_1(x) \left(\frac{x}{a^2} - \frac{1}{\sqrt{a^2 - x^2}} \arccos \frac{x}{a} \right). \quad (43)$$

Numerical integration of Eq. (43) gives

$$\Delta E_x = -0.25 \frac{e N_e \Delta x}{a^2}. \quad (44)$$

Comparing this result with Eq. (38) we see that the factor κ is approximately equal to $1/16$.

Equation (44) gives the electric field acting on the next bunch that follows the displaced one. Subsequent bunches will feel a smaller perturbation because, as was shown in Section 4, the number of electrons is decaying with the lifetime given by Eq. (24). This means that the perturbation of the electron cloud will exponentially decay in time together with the electric field, $\Delta E_x \propto \exp(-tq/t_{\text{sep}})$.

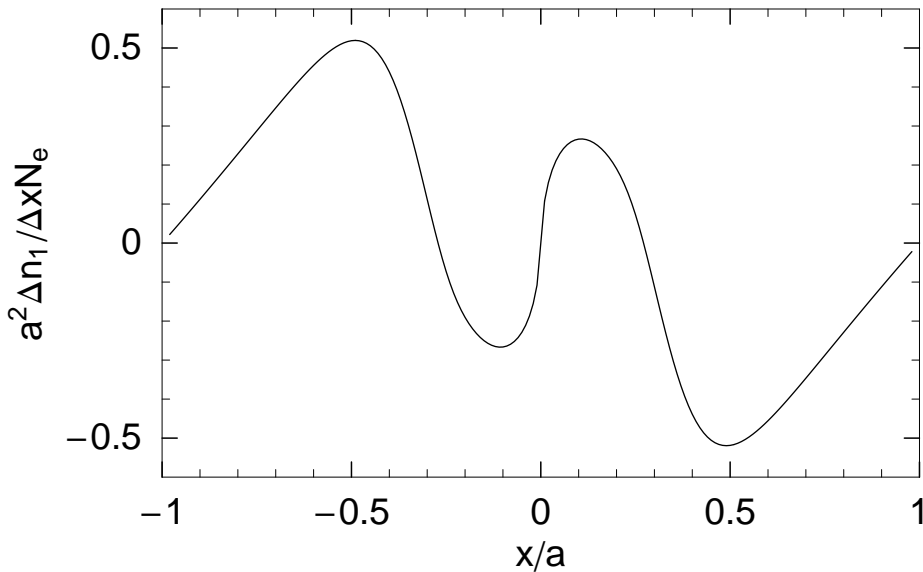


Figure 9: Normalised density perturbation $\Delta n_1(x)a^2/N_e\Delta x$ as a function of x .

Formally, we can introduce a transverse wakefield $w_x(z)$ per unit length of the pipe associated with the interaction of the beam with the electrons,

$$w_x(z) = \frac{\Delta E_x}{N_b e \Delta x} = -0.25 \frac{N_e}{N_b a^2} e^{-zq/L_{\text{sep}}}, \quad (45)$$

which has a dimension of cm^{-3} . However, in contrast to usual wakes describing an electromagnetic interaction of the beam with elements of the vacuum chamber, the wake (45) depends on the number of particles in the bunch.

Using Eq. (45) we can find a growth rate of the multibunch instability. The derivation in Appendix B gives

$$\gamma_{\text{max}} = \frac{N_b r_p c^2 |w_0|}{4q\gamma\omega_\beta} = 0.06 \frac{N_e r_e c^2}{qa^2\gamma\omega_\beta}, \quad (46)$$

where $w_0 = w_x(0)$. Assuming $q = 0.2$, this formula reduces to Eq. (39) with a factor $\kappa \approx 0.1$. For the parameters used in Section 8.1, we find the instability growth time $\tau_{\text{inst}} \approx 180$ msec.

9 Discussion

In this paper, we developed a semi-analytical model of electron cloud build-up in the LHC. The model is based on several assumptions which are made to simplify the treatment. The most critical assumptions, in our opinion, are using the kick approximation for the energy gain, Eq. (18), and an approximate treatment of the effect of the electric field in Section 5. Using the first assumption, we somewhat overestimate the energy gain for the electrons close to the beam. However, due to a slow variation of the secondary electron coefficient at energies above W_0 (see Fig. 2), the result is not sensitive to energy errors in

this range. Our second assumption allows an analytic solution for the distribution function in the regions without magnetic field. Assuming a constant electric field within the cloud it correctly treats the dynamics of the electrons near the wall only. These are electrons with the smallest kinetic energy for which the effect of the electric field is dominant. Faster electrons that quickly reach the central region of the pipe are not treated correctly by this model, however, due to their larger kinetic energy the effect of the electric field for them is relatively weak. Overall, we believe that even with these (and other simplifications) our model gives a reasonably good description of the beam dynamics and, what is most important, establishes the main dependencies between different parameters.

We found two different regimes for the development of the electron cloud. If the system is below the multipacting condition, the density of each group of electrons produced by a single bunch exponentially decays with time. After a transient period during passage of several bunches, the density of the electron cloud reaches an equilibrium level given by Eq. (23); typically, this is several times larger than the electron density produced by a single bunch.

If the system gets into the multipacting regime, the density of each individual group of electrons grows exponentially until stopped by the space charge effect. In this regime, the electron density (and the energy deposition to the wall) is several times higher than without multipacting.

We also studied two dynamical effects caused by the electron cloud. One is the emittance growth of the proton beam due to the interaction with a random component of the electric field generated by electrons. Although our estimate gives an emittance doubling time large enough not to be a concern, the effect cannot be completely discarded because of uncertainty involved in the choice of the correlation length of the random field. Another important effect associated with the cloud is the multibunch instability due to the wakefield produced by the electrons. We calculated the wake function and found the growth rate of the instability of the order of 0.2 s.

The ways to improve the situation with electrons are rather obvious. Reducing the secondary emission coefficient (with the help of a special surface treatment or coating) to a level below multipacting would be the most radical solution of the problem. In addition, lowering the reflectivity of the surface (by increasing the surface roughness ⁸⁾) would lead to absorption of photons in a narrow horizontal strip where the motion of electrons is limited by the magnetic field such that the secondary emission is effectively suppressed. Another choice, that would unfortunately lead to a deterioration of the machine performance, could be increasing the bunch distance. Our calculations show that a twofold increase of the bunch distance, from 7.5 m to 15 m, would lead to an increase of the minimal value of δ_{crit} from 1.3 to 2.3. Another possibility of increasing δ_{crit} by lowering the beam current turns out not to be effective: calculations show that a fivefold lowering of the current down to 0.1 A would only increase δ_{crit} from 1.3 to 1.6.

The mathematical code of this model is implemented as a Mathematica 3.0 notebook and is available on the World Wide Web site <http://wwwslap.cern.ch/collective/electron-cloud/>.

⁸⁾ The most recent measurements showed that the reflectivity at 11 mrad incidence angle for an average surface roughness of 1.6 μm is only 5%, [12].

Acknowledgements

I would like to thank Francesco Ruggiero for many illuminating discussions during the course of this work and a careful reading of the manuscript. I am thankful to Oliver Brüning for sharing results of his computer simulations and stimulating discussions and to J. S. Berg and R. Talman for critical remarks concerning the beam emittance growth.

I also want to thank the AP group of the CERN SL division, in particular Francesco Ruggiero, Jacques Gareyte, for the invitation to CERN, hospitality and support.

References

- [1] F. Zimmermann, "A Simulation Study of Electron-Cloud Instability and Beam-Induced Multipacting in the LHC", CERN LHC Project Report 95 (1997); SLAC-PUB-7425 (1997).
- [2] M. Furman, "The Electron-Cloud Effect for LHC", Proceedings of the International Workshop on Multibunch Instabilities in Future Electron and Positron Colliders, Tsukuba, Japan, 1997.
- [3] O. Gröbner, "Beam Induced Multipacting", Proceedings of PAC97, Vancouver, Canada, May 1997; LHC Project Note 127 (1997).
- [4] O. Brüning, "Simulation for the Beam-Induced Electron Cloud in the LHC Liner", LHC Project Note 102 (1997).
- [5] A. V. Burov and N. S. Dikansky, "Electron-Cloud Instabilities", Proceedings of the International Workshop on Multibunch Instabilities in Future Electron and Positron Colliders, Tsukuba, Japan, 1997; World-wide web page <http://wwwslap.cern.ch/collective/electron-cloud>.
- [6] O. Gröbner, 10th Int. Conference on High Energy Accelerators, Protvino (1977).
- [7] The Large Hadron Collider, Conceptual Design, CERN/AC/95-05 (1995).
- [8] World-wide web page 'http://www-crxo.lbl.gov/optical_constants/' published by the LBNL X-ray laboratory.
- [9] F. Ruggiero, private communication, September 1997.
- [10] S.A. Heifets, "Transverse Instability Driven by Trapped Electrons", SLAC/AP-95-101 (1995).
- [11] J. S. Berg, "Energy Gain in an Electron Cloud During the Passage of a Bunch", LHC Project Note 97 (1997).
- [12] F. Ruggiero, private communication, September 1997.
- [13] H. Seiler, "Secondary electron emission in the scanning electron microscope", J. Appl. Phys. 54 (11) (1983).
- [14] R. J. Goldston and P. H. Rutherford. Introduction to Plasma Physics, (Institute of Physics Publishing, Bristol), 1995.
- [15] V. Lebedev, V. Parkhomchuk, V. Shiltsev and G. Stupakov. Particle Accelerators, vol. 44, p. 147 (1994).
- [16] K. Ohmi, Phys. Rev. Lett., Vol. 75, No. 8 (1995).
- [17] A. Chao, "Physics of Collective Beam Instabilities in High Energy Accelerators", Wiley, p. 208 (1995).

Appendix A

In this Appendix we calculate the electric field on the pipe axis generated by an electron cloud with density $\Delta n_e(x)$ which does not depend on y and z .

Using a complex notation, $z = x + iy$ and a complex electric field $E_x + iE_y$ it is easy to check that the Green function corresponding to the electric field of an infinitely

thin charged wire stretched parallel to a circular pipe axis at x_0, y_0 with charge per unit length σ is given by the following formula:

$$E_x(x, y) + iE_y(x, y) = 2\sigma \left(\frac{1}{\bar{z} - \bar{z}_0} - \frac{1}{\bar{z} - \bar{z}_i} \right), \quad (47)$$

where the bar denotes a complex conjugate variable, and $\bar{z}_i = a^2/z_0$ gives the image charge location. We are interested in the electric field at the center of the pipe, $z = 0$. This reduces Eq. (47) to

$$E_x + iE_y = 2\sigma \left(\frac{x_0 + y_0}{a^2} - \frac{1}{x_0 - iy_0} \right). \quad (48)$$

Using this Green function, we can find the electric field for and an arbitrary density $\Delta n_e(x)$ (it is evident that the E_y component on the axis vanishes if Δn_e does not depend on y)

$$\begin{aligned} E_x &= -2e \int_{-a}^a dx_0 \int_{-\sqrt{a^2-x_0^2}}^{\sqrt{a^2-x_0^2}} dy_0 \Delta n_e(x_0) \left(\frac{x_0 + y_0}{a^2} - \frac{1}{x_0 - iy_0} \right) \\ &= -4e \int_{-a}^a dx_0 \Delta n_e(x_0) \left(\frac{x_0}{a^2} \sqrt{a^2 - x_0^2} - \arccos \frac{x_0}{a} \right), \end{aligned} \quad (49)$$

where we took into account that electrons have negative charge $-e$.

Appendix B

Following Ref. [17], we derive here the growth rate of a multibunch instability with a wake function given by Eq. (45).

The equation of motion for the n th bunch is

$$\Delta \ddot{x}_n + \omega_\beta^2 \Delta x_n = \frac{N_b r_p c^2}{\gamma} \sum_{m=0}^{M-1} w_x ((m-n)L_{\text{sep}}) \Delta x_m (t - (m-n)t_{\text{sep}}), \quad (50)$$

where ω_β is the betatron frequency, M is the number of bunches in the ring, and the dot indicates the time derivative.

Assuming harmonic dependence in time,

$$\Delta x_n = \tilde{x}_n e^{-i\omega t}, \quad (51)$$

we find

$$(\omega_\beta^2 - \omega^2) \tilde{x}_n = \frac{N_b r_p c^2}{\gamma} \sum_{m=0}^{M-1} \tilde{x}_m w_x ((m-n)L_{\text{sep}}) e^{i\omega(m-n)t_{\text{sep}}}. \quad (52)$$

Typically, correction to the frequency due to the instability is much smaller than ω_β . This allows us to simplify the left hand side of Eq. (52) and use ω_β in the exponentiation factor on the right hand side

$$(\omega - \omega_\beta) \tilde{x}_n = -\frac{N_b r_p c^2}{2\gamma\omega_\beta} \sum_{m=0}^{M-1} \tilde{x}_m w_x ((m-n)L_{\text{sep}}) e^{i\omega_\beta(m-n)t_{\text{sep}}}. \quad (53)$$

We specify a multibunch mode by an index μ , $0 < \mu < M - 1$, such that

$$\tilde{x}_m \propto e^{2\pi i \mu m / M}, \quad (54)$$

which immediately gives a growth rate for the μ th multibunch mode

$$\gamma_\mu = -\frac{N_b r_p c^2}{2\gamma\omega_\beta} \text{Im} \sum_{k=1}^{\infty} w_x(kL_{\text{sep}}) e^{k(i\omega_\beta t_{\text{sep}} + 2\pi i\mu/M)}, \quad (55)$$

where we took into account that due to a rapid exponential decay of the wake function the summation can be extended up to infinity.

Rewriting Eq. (45) in the form

$$w_x(kL_{\text{sep}}) = w_0 e^{-kq}, \quad (56)$$

and performing summation in Eq. (55) we find

$$\sum_{k=1}^{\infty} w_x(kL_{\text{sep}}) e^{k(i\omega_\beta t_{\text{sep}} + 2\pi i\mu/M)} = w_0 \frac{e^{-q+i\omega_\beta t_{\text{sep}}+2\pi i\mu/M}}{1 - e^{-q+i\omega_\beta t_{\text{sep}}+2\pi i\mu/M}}. \quad (57)$$

Assuming that $q \ll 1$ and $\mu/M \ll 1$ (and also using the fact that $\omega_\beta t_{\text{sep}} \ll 1$), we can expand expression (57) and find the maximum of the growth rate

$$\gamma_{\text{max}} = \frac{N_b r_p c^2 |w_0|}{4q\gamma\omega_\beta}. \quad (58)$$